ORBITAL SOLUTIONS TO LEO-TO-LEO ANGLES-ONLY VERY-SHORT-ARC TRACKS

Jizhang Sang[(1)], Xiangxu Lei[(2)], Pin Zhang[(3)], Teng Pan[(4)], Huaifeng Li [(5)]

[(1)]*School of Geodesy and Geomatics, Wuhan University, Wuhan, China, email: jzhsang@sgg.whu.edu.cn*

[(2)]*School of Geodesy and Geomatics, Wuhan University, Wuhan, China, email: xxlei@whu.edu.cn*

[(3)]*School of Geodesy and Geomatics, Wuhan University, Wuhan, China, email: pzhang1992@whu.edu.cn*

[(4)]*China Academy of Space Technology, Haidian District, Beijing, China, email: panteng@cast.cn*

[(5)]*China Academy of Space Technology, Haidian District, Beijing, China, email: 25289492@qq.com*

ABSTRACT

Two critical problems are encountered in the space-based LEO-to-LEO optical tracking of new space debris. The first is the initial orbit determination (IOD) from angles of a very short-arc (VSA). The second problem is the association between the IOD results. To the first problem, a range-search method is applied to tackle the LEO-to-LEO VSA angles-only IOD problem. The method assumes ranges at two chosen epochs and then the Lambert problem is solved where a residual control process is employed to control the IOD solutions. Then, a geometrical approach, which only uses an analytical orbital propagator, to associating the LEO-to-LEO uncorrelated tracks (UCTs), is developed. The procedure are experimented with simulation data and very encouraging results are obtained.

1 INTRODUCTION

The orbital arc length from the optical observation of low Earth orbiting (LEO) objects from a LEO spacecraft would usually be about 10~20s when the tracking telescope operates in the scan (satellite-body fixed) mode. In case that a new object is detected from the very short-arc (VSA) angles, the obtained angles will be processed using an initial orbit determination (IOD) algorithm to determine a set of orbital elements, but the errors of the determined elements are usually very large. A single track from this process is essentially of little value if it cannot be associated to another track from the same object.

The traditional Gauss, Laplace IOD methods or their variants[1], suffer from the poor geometrical strength provided by the VSA angles and thus have problem to achieve a converged solution. The more recent Gooding method[2] would need appropriate initial values of the ranges between the observing and observed objects for the convergence. Even a convergence is achieved with these methods, the solutions usually have very large errors. An imminent first step is to find an algorithm of high success rate to obtain an IOD solution when only the LEO-to-LEO VBA angles are available. Such a single IOD solution for a new object is the so-called uncorrelated track (UCT).

Given a UCT, one has to associate it to other UCTs to make them useful for the object cataloguing. Various association methods have been proposed [e.g., 3-6]. In all these methods, a distance-like metric is computed from the propagated IOD orbits of two UCTs and their uncertainties to measure the closeness between them. There are two challenges in the process: the availability of the uncertainties and the propagation of the uncertainties. The existing track association methods are theoretically sound, but may be difficult to use in the case of the LEO-to-LEO VSA UCT association, simply due to the unavailability of, or large errors in, the covariance of the IOD tracks. An alternative approach using only the IOD orbital elements would be practically more attractive, and in some cases demanding.

The space-based VSA angles-only IOD and UCT association are two of the most critical steps in building a space object catalogue. This paper presents the main ideas on the two subjects being proposed in the development of a comprehensive software of building and maintaining a space object catalogue using the space-based optical tracking, as well as some simulation results.

2 RANGE-SEARCH BASED IOD

2.1 Method basics

Given a set of right ascensions and declinations of an observed object $(RA_1, Dec_1, t_1; \ldots; RA_n, Dec_n, t_n)$ at n epochs at which the locations of the observer are known. The unit vector at t_i from the observer to the object is

$$\boldsymbol{L}_i = \begin{bmatrix} L_{xi} = \cos(Dec_i)\cos(RA_i) \\ L_{yi} = \cos(Dec_i)\sin(RA_i) \\ L_{zi} = \sin(Dec_i) \end{bmatrix} \quad (1)$$

The whole arc is now divided into an IOD arc from t_1 to t_k and a control arc from t_{k+1} to t_n. Assume that the ranges at t_1 and t_k are ρ_1 and ρ_k, respectively, and the

positions of the observer at t_1 and t_k are $\boldsymbol{r}_1$ and $\boldsymbol{r}_k$, respectively. The positions of the object at t_1 and t_k are then $\boldsymbol{R}_1 = \boldsymbol{r}_1 + \rho_1 \boldsymbol{L}_1$ and $\boldsymbol{R}_k = \boldsymbol{r}_k + \rho_k \boldsymbol{L}_k$, respectively. In this way, it is now the Lambert problem of IOD, and a set of Kepler orbital elements could be computed. By stepping through the sufficiently large search ranges for ρ_1 and ρ_k, it is possible to obtain some solutions close to the truth.

2.2 Quality control

For each converged solution from the Lambert problem, a quality control process is performed to decide whether the solution is an acceptable one. The first check is on the eccentricity which has to be greater than 0 to ensure the orbit is of an Earth orbiting object. Then, the perigee altitude of the orbit should be at least 0.

Next, the angles in the control arc are used in the solution quality control. The IOD elements are propagated to an observing epoch t_i $(k+1 \le i \le n)$, and the position of the object is computed. Together with the known position of the observer at t_i, the right ascension and declination, $(\widetilde{RA}_i, \widetilde{Dec}_i)$ are computed. They are differenced with the observed ones, resulting in the residuals of the computed $(\widetilde{RA}_i, \widetilde{Dec}_i)$:

$$\Delta RA_i = \left(\widetilde{RA}_i - RA_i\right) \cos Dec_i \qquad (2)$$

$$\Delta Dec_i = \widetilde{Dec}_i - Dec_i \qquad (3)$$

It is clear that, if the estimated IOD orbit is close to the truth orbit, the residuals will be small. The magnitudes and the variation trend of the residuals will be good indicators of the closeness between the IOD orbit and its truth. Three metrics can be determined from the residuals of either the right ascension or the declination: the mean, the RMS and the slope of the residuals. A set of IOD elements is accepted as a candidate solution to the VSA angles-only IOD problem if the three metrics of both the right ascension and declination are less than pre-set thresholds.

2.3 Determination of final solution

There are could be multiple, and many in some cases, candidate solutions, depending on the values of the thresholds. It is necessary to find a set of elements as the final solution to the VSA IOD problem. For the near-circular orbits, the procedure is described below, assuming there are l solutions $\{a_j, e_j, i_j, \Omega_j, \omega_j, M_j; j = 1,2,\dots,l\}$.

1. Determination of the eccentricity. Choose the solutions whose eccentricities are among the smallest 10% of all eccentricities. The average of these 10% eccentricities is then regarded as the final eccentricity, e.
2. Determination of the SMA. Find all a_j from l SMAs each of which satisfies $\left|e_j - e\right| < D_e = 10^{-5}$, and then regard the average of all these a_j as the final SMA, a.
3. Determination of perigee argument and mean anomaly. Find all ω_j from l perigee arguments each of which satisfies $\left|a_j - a\right| < D_a = 10000m$, and then regard the average of all these ω_j as the final perigee arguments, ω; and the average of the corresponding M_j as the final mean anomaly, M.
4. Determination of the inclination and right ascension of the node. Take the median of all the inclinations as the final inclination, i; and similarly, take the median of all the right ascensions of the node as the final right ascension of the node, Ω.

3 IOD UCT ASSOCIATION BY ADJUSTMENT OF SEMI MAJOR AXIS

3.1 Basic theory

The proposed method only uses the position difference, expressed in the along-track, cross-track and radial (ACR) directions, between two tracks. By examining the relationship between the ACR difference and the variation of the semi major axis (SMA), it would be possible to find some insights into the proposed method. Since the SMA is the most difficult and important element to be estimated from VSA angles, and its error has accumulating effect on the along-track bias, the discussion is focused on the effect of the SMA error on the ACR difference,

Assume there are two sets of Keplerian orbit elements at two epochs, each representing an initial orbit track. If the elements are exact, then the ACR difference between the two tracks is zero. When there are errors in the elements, the ACR differences will vary as a function of time and the error magnitudes. Figure 1 demonstrates the ACR differences against the orbit element errors, where the two sets of reference orbit elements are given in Table 1. Figures 1(1) to 1(3) show the ACR differences over one day due to errors of 0.005, 0.3 degrees and 0.5 degrees, respectively, in the eccentricity, inclination and perigee argument of Track 1. When the SMA of Track 1 has an error of 10 km, the resulting differences are shown in Figure 1(4). The combined differences are shown in Figure 1(5). It is clearly seen that, over the time period of one day, the differences in Figures 1(1) to 1(3) are mainly periodic and remain bounded, while the along-track and radial differences in Figure 1(4) grow with the time from the reference epoch of Track 1.

When the elements of both tracks have errors, the behaviour of the differences caused by the errors in the non-SMA elements are generally unchanged, as shown in Figure 2. In Figure 2(1), the ACR differences are

generated by adding 0.005 and -0.002, respectively, to the reference eccentricities of Track 1 and Track 2. Figure 2(2) are for the ACR differences due to the errors of 0.3 and -0.1 degrees, respectively, in the reference inclinations. Figure 2(3) shows the ACR differences caused by the errors of 0.5 and -0.5 degrees, respectively, in the reference perigee arguments.

However, the differences between the two tracks due to the SMA errors have various variation patterns. Assume the SMA of Track 1 has an error of 10km, and the SMA of Track 2 has errors of 30km, 10km, -10km and -30km, respectively, the ACR differences are shown in Figures 2(4) to 2(7). It can be seen that when the SMA errors of the similar magnitude but opposite sign, the position differences will have a near-zero value, such as in Figure 2(6).

A further investigation into the variation pattern reveals that, when the SMAs of the tracks have errors of the same magnitude but opposite sign, the along-track biases approach zero near the middle of the two reference epochs, as shown in Figure 3, where the SMA errors of the two tracks vary from -150km to 150km.

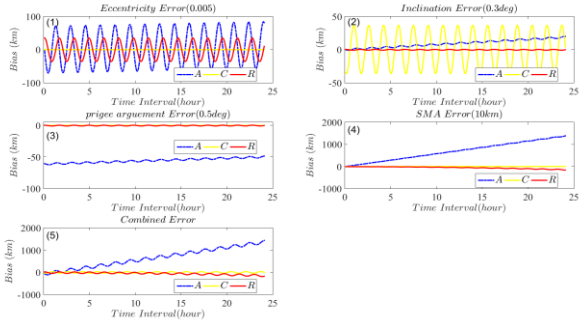

Figure 1: ACR Differences with different errors of Track 1

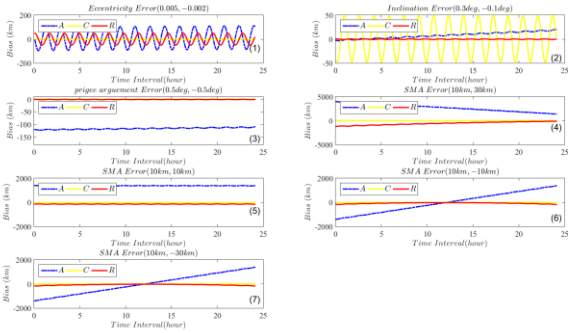

Figure 2: ACR differences when elements of both track have errors

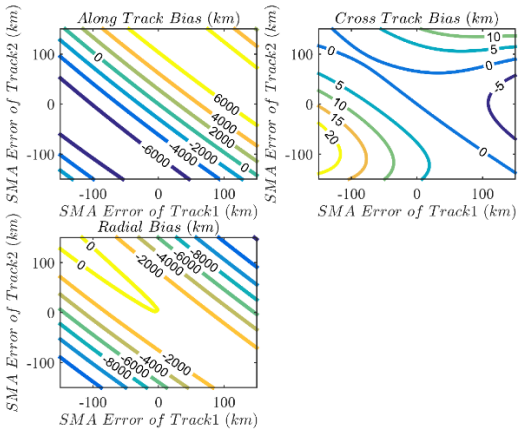

Figure 3: ACR differences with different SMA errors of Track 1 and Track 2

Table 1: Reference Keplerian elements

	Track 1	Track 2
Reference time	2017.01.01	2017.01.02
	0h0m0s	0h0m0s
Semi-major axis (km)	7000	7012.8
Eccentricity	0.01	0.011
Inclination (deg)	60.0	60.0
Right asc. of the node (deg)	120	116.4
Perigee argument (deg)	70	66.3
Mean anomaly (deg)	0	-66.3

The theory behind this property can be explained as follows. The accumulative along-track bias is predominantly caused by the errors in the mean motion, n, which is related to the SMA, a, through the following equations:

$$n^2 a^3 = \mu \qquad (4)$$

$$\Delta n = -3n \cdot \Delta a/2a \qquad (5)$$

where μ is the gravitational constant of the Earth, Δa and Δn are the errors of the SMA and mean motion.

For a near circular orbit, the change in the along-track difference from one epoch to another due to the mean motion error can be approximated by

$$\Delta l \approx \Delta n \cdot (t_2 - t_1) \cdot a, \quad t_2 \geq t_1 \qquad (6)$$

Now, it is assumed that the mean motions of two tracks at reference epochs T_1 and T_2 have errors Δn_1 and Δn_2, respectively, and the SMAs of both tracks are regarded as the same, it is easy to have the following equations for

the changes in the along-track differences due to Δn_1 and Δn_2:

$$\Delta l_1 \approx \Delta n_1 \cdot (t - T_1) \cdot r$$

$$\Delta l_2 \approx \Delta n_2 \cdot (t - T_2) \cdot r$$

where r is the geocentric distance of the space object at time t. The combined change in the along-track difference at epoch t, Δl_t, is the sum of Δl_1 and $-\Delta l_2$, where the minus sign is needed for Δl_2 to account for the direction of the along-track difference.

Let t_m be the middle of T_1 and T_2,

$$t_m = (T_1 + T_2)/2$$

then,

$$\Delta l_{t_m} = (\Delta n_1 + \Delta n_2)(t_m - T_1) \cdot a \qquad (7)$$

From Eq. (7), the condition for the zero value of the combined effect in the along-track difference at the middle epoch is obtained as

$$\Delta n_1 = -\Delta n_2 \qquad (8)$$

The equivalent condition is therefore:

$$\Delta a_1 = -\Delta a_2 \qquad (9)$$

Eq. (9) says, when the errors of the SMAs in the two tracks have the same magnitude but opposite sign, the combined change in the along-track difference at the middle epoch is zero. This agrees with the findings from Figure 2.

In practice, the errors of the SMAs of the two tracks are unknown. Δl_{t_m} is computed from the propagated positions of the two tracks. Let the estimated SMAs of the two tracks be a_1 and a_2, respectively, an approximate expression for Δl_{t_m} would be obtained as

$$\Delta l_{t_m} \approx \Delta n (t_m - T_1) \cdot r_m \qquad (10)$$

where

$$\Delta n \approx -\frac{3n_m}{2a_m}(a_1 - a_t + a_2 - a_t)$$

$$= -\frac{3n_m}{2a_m}(\Delta a_1 + \Delta a_2)$$

$$a_m = (a_1 + a_2)/2$$

$$n_m = \sqrt{\mu / a_m^3}$$

where a_t is the true SMA of the track, which is unknown. From Eqs. (7) and (9), one can see that, when $\Delta a_1 = -\Delta a_2$, Δl_{t_m} becomes zero. More importantly, $\Delta l_{t_m} = 0$ means $\Delta a_1 + \Delta a_2 = 0$, and an estimate of the true SMA of the track can be obtained as

$$a_t = (a_1 + a_2)/2$$

If $\Delta l_{t_m} \neq 0$, it is possible to adjust one of the two SMAs to make $\Delta l_{t_m} = 0$. The adjusted value in the SMA, δa, is determined as

$$\delta n = \frac{\Delta l_{t_m}}{(t_m - T_1) \cdot r_m} \qquad (11)$$

$$\delta a = -\frac{2}{3}\frac{a_m}{n_m}\delta n \qquad (12)$$

Finally, an estimate of the true SMA of the track can be obtained as

$$\tilde{a}_t = (a_1 - \delta a + a_2)/2 \qquad (13)$$

3.2 Case studies

Two examples are presented here to demonstrate the effect of adjusting the SMA of Track 1 on the ACR difference at the middle epoch. The first example is about two tracks from a same LEO object, which is observed twice, apart by 28h 35m, by a LEO-based optical system in scanning mode. The estimated IOD elements and their true elements are given in Table 2. It is seen that the IOD elements have very large errors. The along-track, cross-track and radial differences after each adjustment of the SMA are shown in Table 3.

After the propagations of the two IOD element sets to the middle epoch, the ACR differences between the two tracks are computed from the 3-dimensional position and velocity vectors. The initial differences are -854.6km, -6.0km and -108.5km, respectively. Then, the adjusted value in the SMA is computed from Eqs. (11) and (12). And the use of Eq. (13) gives a SMA estimate of 7794.9 km, which differs with the true values at the reference epochs of Track 1 and Track 2 by only 2.5 km and 0.9 km, respectively, while the initial errors are about 18 km and 27 km, respectively, as Table 3 shows.

The newly estimated SMA is used to replace the SMA of Track 1, and the above computation is repeated, which results in new ACR values shown in the row of "Second adjustment" in Table 3, and they are significantly smaller than those in the "First adjustment" row. A new SMA estimate of 7994.8 km is obtained, and the third adjustment is performed, which results in a new set of ACR values, where the along-track difference is close to zero. These results show that the along-track difference decreases gradually with the SMA adjustment of Track 1 while the radial and cross-track differences may vary inconsistently.

The second example is about the ACR difference variations between two tracks from different LEO objects, with the orbit elements listed in Table 4. The ACR values after each SMA adjustment are shown in Table 5.

From Table 5, it is seen that the along-track differences

gradually decrease after each SMA adjustment, but it does not approach to zero after the third adjustment. The SMA estimates are not close to either the true SMA values of the two tracks or their average. In addition, the cross-track and radial differences in the "First adjustment" row are much larger than those in the first example, and their changes are inconsistent. This example demonstrates that, when the SMAs are adjusted, the properties of ACR values between two tracks from different LEO objects are quite different from the properties when the tracks are from a same object.

Table 2: Elements of two IOD tracks of a same LEO object

	Track 1		Track 2	
	True	IOD estimate	True	IOD estimate
Reference time	2014.11.15	2014.11.15	2014.11.16	2014.11.16
	14h5m6s	14h5m6s	18h40m57s	18h40m57s
SMA (km)	7792.4	7810.7	7794.0	7767.1
Eccentricity	0.0006	0.0027	0.0009	0.0029
Inclination (deg)	82.57	81.97	82.57	82.15
RAAN (deg)	131.78	131.97	131.02	131.02
Perigee (deg)	30.39	332.35	34.54	257.82
Mean Anomaly (deg)	312.47	10.39	314.97	99.14

Table 3: Orbit biases at middle epoch after SMA adjustments of two tracks from a same object

	A (km)	C (km)	R (km)	Estimated SMA (km)	True SMA1 (km)	True SMA2 (km)
First adjustment	-854.6	-6.0	-108.5	7794.9	7792.4	7794.0
Second adjustment	14.3	-13.4	-22.8	7794.8	7792.4	7794.0
Third adjustment	0.06	-13.3	-22.8	7794.8	7792.4	7794.0

Table 4: Elements of two IOD tracks from two different LEO objects

	Track 1		Track 2	
	True	IOD estimate	True	IOD estimate
Reference time	2014.11.17	2014.11.17	2014.11.17	2014.11.17
	5h55m33.1s	5h55m33.1s	17h44m30.2s	17h44m30.2s
SMA (km)	7489.8	7448.6	7501.3	7451.0
Eccentricity	0.0065	0.0015	0.0077	0.0017
Inclination (deg)	100.5	100.50	100.54	100.93
RAAN (deg)	59.25	59.24	57.68	57.25
Perigee (deg)	142.41	232.97	176.60	222.49
Mean Anomaly (deg)	348.82	259.20	313.48	267.20

Table 5: Orbit biases at the middle epoch after SMA adjustments of two tracks from different tracks

	A (km)	C (km)	R (km)	Estimated SMA (km)	True SMA1 (km)	True SMA2 (km)
First adjustment	-7286.0	53.163	-6388.5	7356.1	7489.8	7501.3
Second adjustment	-3033.6	-107.6	-676.3	7242.2	7489.8	7501.3
Third adjustment	-89.4	-168.6	-5.5	7195.8	7489.8	7501.3

3.3 Algorithm implementation

Following the above method developments and case studies, the procedure to implement the UCT association algorithm can be described. Given a pair of IOD UCTs, IOD_i and IOD_k, the task is to determine whether they are of a same object. The association will result in one of four solutions:

(1) true positive (TP), the two IOD UCTs are of a same object, and the solution says they are of a same object;

(2) true negative (TN), the two IOD UCTs are of a same object, but the solution says they are of two objects;

(3) false positive (FP), the two IOD UCTs are of two objects, but the solution says they are of a same object;

(4) false negative (FN), the two IOD UCTs are of two objects, and the solution says they are of two objects.

A good algorithm should have high TP and FN rates.

The algorithm to determine whether two IOD UCTs are associated is implemented as:

1. If the reference epochs of IOD_i and IOD_k are apart by more than 3 days, no association decision is made.
2. Propagate IOD_i and IOD_k to the middle epoch with the analytical orbit propagator [7] and the resulting orbit elements (IOD_{im} and IOD_{km}) are obtained.
3. Compare the SMAs of IOD_{im} and IOD_{km}, if they differ by more than 300km, IOD_i and IOD_k are judged not from a same object.
4. Compute the angle between the normal vectors of the two orbital planes at the middle epoch, if the angle is larger than 3 degrees, IOD_i and IOD_k are judged not from a same object.
5. Compute the ACR differences at the middle epoch between IOD_{im} and IOD_{km}.
6. Compute the mean motions n_i and n_k from IOD_i and IOD_k to obtain $n_m = (n_i + n_k)/2$.
7. Compute r_i and r_k at the middle epoch to obtain $r_m = (r_i + r_k)/2$.
8. Compute δa using Eqs. (11) and (12).
9. Compute a SMA estimate using Eq. (13).
10. Replace the SMAs of IOD_i and IOD_k with the estimated SMA in Step 9, and repeat Steps 2 to 9 for two more times.
11. Compare the last ACR differences with the preset thresholds to determine whether the two IOD UCTs are associated. If the three ACR biases are all less than the corresponding thresholds, a true positive decision is made. Tentative thresholds for the simulation experiments in this paper are 200km, 600km and 600km for the along-track, cross-track and radial differences, respectively.

4 SIMULATION RESULTS

4.1 Generation of tracks

About 2000 LEO objects are selected from the NORAD catalogue for the generation of simulated tracking angles. The tracking spacecraft is at an orbit of altitude 808.6km and inclination 99.82 degree. The orbit determination and analysis software for Earth-orbiting objects [8] is used to generate the "truth" orbits of the 2000 objects and the tracking spacecraft, and angles data of the 2000 objects observed by the tracking spacecraft. The software has the following main functions: orbit determination using various tracking data and considering various perturbing forces, orbit and tracking data simulations, atmospheric mass density calibration, and space conjunction analysis. During November 15-18, 2014, 3077 very-short arcs with duration between 10s and 60s are generated. Most of the durations range from 10s to 20s. The angles data is corrupted by random errors of zero mean and 2" standard deviation.

The corrupted angles data of each of the 3077 arcs is processed through the IOD method presented in Section 2, and 2515 IOD tracks are obtained. A summary of the IOD SMA errors is given in Table 6. It is seen that only 19.6% of the estimated IOD SMAs have errors less than 10 km and 38.6% of them have errors less than 25 km.

Table 6: Statistics of the estimated SMA errors

<10km	10-25km	25-50km	50-100km	>100km
19.6%	19.0%	17.3%	18.4%	25.7%

4.2 UCT association results

Using the method described in Section 3, an all-to-all track associations are performed, and the results are given in Table 7. Only when two IOD tracks are less than 3 days apart, their association is judged. The association results when the track separation is less than two days and one day are also listed to assess the dependence of the algorithm effectiveness on the track separations. In the table, all the rates of true positive, true negative, false positive and false negative are presented to give a complete picture of the algorithm effectiveness.

The proposed method is implemented using C++ in the Microsoft VS2013 environment running on an ASUS laptop computer (Intel (R) Core (TM) i7-4710HQ CPU @ 2.50GHz). The computation time to complete the associations of 2515 IOD tracks is about 206s.

It is found that, when the track separation is less than 3 days, there are 3204 IOD pairs from a same object. 3004 pairs are successfully associated to a same object, representing a true positive rate of 93.8%. On the other hand, 2775026 IOD pairs from two objects can be formed, and 10309 pairs are falsely associated to a same object, representing a false negative rate of 0.4%. From the table, it is also found that the true positive rate increases with the decrease of the track separation, suggesting the algorithm is more effective for associating the IOD tracks with shorter separation.

An analysis is made on the relation between the true positive rate and the magnitude of the IOD SMA error. It would reveal whether the algorithm is able to cope with the situation of large SMA errors. The true positive rates for various IOD SMA error ranges are given in Table 8. It can be seen that, when the SMA errors of two same-object originated IOD tracks are both less than 50 km, they can be successfully associated with a true positive rate of 100%. When the SMA errors of two same-object originated IOD tracks are both less than 100 km, the true positive rate is higher than 92%. When the SMA error of one IOD is larger than 100 km and other is between 25-100 km, the true positive rate is between 74% and 85%. Generally, this table demonstrates that the true positive rate increases with the decrease of the SMA error of IOD, suggesting the algorithm is more effective for associating the tracks with lesser SMA error.

In addition to the track association capability, the algorithm is also able to generate a new estimate of the SMA if the two tracks are of a same object. Table 9 presents the statistics of the estimated SMA errors after the true positive association of tracks with separation less than 3 days. It shows that the estimated SMA error is much smaller than the initial ones. In particular, 68.5% and 82.5% of the estimated SMAs have errors less than 5km and 10 km, respectively, a significant improvement on the initial 8.8% and 19.6%.

Table 7: Track association results

Track separation	<3 day		< 2 day		< 1 day	
IOD pairs from a same object	3204		2392		1118	
True positive	3004	93.8%	2309	96.5%	1114	99.6%
True negative	200	6.2%	83	3.5%	4	0.4%
IOD pairs from two objects	2775026		1994513		806429	
False positive	10309	0.4%	7682	0.4%	3374	0.4%
False negative	2764717	99.6%	1986831	99.6%	803055	99.6%

Table 8: True positive rates (%) for different IOD SMA errors

	<10km	10-25km	25-50km	50-100km	>100km
<10km	100.0	100.0	100.0	100.0	100.0
10-25km	100.0	100.0	100.0	100.0	88.5
25-50km	100.0	100.0	100.0	100.0	77.3
50-100km	100.0	98.3	98.8	92.0	84.9
>100km	96.0	80.0	74.4	74.2	85.5

Table 9: Statistics of the estimated SMA errors after the true positive track association

	<1km	<5km	<10km	<25km	<50km	<100km	>100km
Initial	1.4%	8.8%	19.6%	38.6%	55.9%	74.3%	25.7%
New estimate	15.5%	68.5%	82.5%	88.6%	90.4%	92.0%	8.0%

5 CONCLUSIONS

In the case of space-based optical tracking, only very-short arc angular observations of LEO objects will be collected when the telescope is operated in the scanning mode, and the subsequent IOD process would determine the orbit elements with very large errors, whose magnitudes are usually unknown. Therefore, it would be unable to use the existing orbit track association methods which all require orbit state and its covariance (or probability distribution function). On the other hand, thousands of LEO space-based very-short arcs could be observed over a few days, the computing efficiency of track association has to be considered.

A purely geometrical and computationally efficient method would be practically very useful, and demanding in some cases, for the space-based VSA track association. In this paper, such a method is proposed for the association of space-based VSA tracks of near-circular orbits. The method uses a simple relationship between the along-track difference and SMA error.

The method is experimented for the simulated space-based VSA near-circular LEO IOD tracks. The errors of the determined IOD elements are typically very large, for example, 25% of the SMA errors are larger than 100 km. In general, when time interval between two IOD tracks is less than 3 days, this method has a true positive rate over 93% to associate two IOD tracks belonging to a same object, and a false negative rate over 99% to disassociate two IOD tracks. Even when the SMA errors of one or both tracks are larger than 100 km, the true positive rate is still higher than 74%.

The algorithm is very easy to implement and computationally efficient because only a simple analytical orbit propagator is used.

The future work will be focused on expanding and testing the algorithm to non-circular LEO tracks. It would need to simultaneously adjust the semi major axis and eccentricity in order to minimize both the along-track and radial differences, and at the same time to obtain estimates of the semi major axis and eccentricity. A comparison study between the covariance-based methods and this method is also planned.

6 REFERENCES

1. Escobal, P.R. (1965). *Methods of orbit determination*, New York: Wiley.
2. Gooding, R.H. (1996). A new procedure for the solution of the classical problem of minimal orbit determination from three lines of sight. *Celes. Mech. Dyn. Astron.* **66**(4): 387 – 423.
3. Hill, K., Alfriend, K.T., and Sabol, C. (2008). *Covariance-based uncorrelated track association.* AIAA 2008-7211, AIAA/AAS Astrodynamics Specialist Conference, Honolulu, HI.
4. Maruskin, J.M., Scheeres, D.J., Alfriend, K.T. (2009). Correlation of optical observations of objects in earth orbit. *Journal of Guidance, Control, and Dynamics*, **32**(1): 194 – 209.
5. Fujimoto, K., Alfriend, K.T. (2015), Optical Short-Arc Association Hypothesis Gating via Angle-Rate Information. *Journal of Guidance, Control, and Dynamics*, **38**(9): 1602 – 1613.
6. Hussein, I.I., Roscoe, C.W.T., Schumacher, P.W. Jr., and Wilkins, M.P. (2016), UCT Correlation using the Bhattacharyya Divergence, AAS 16-319, the 26th AAS/AIAA Space Flight Mechanics Meeting, Napa, CA.
7. Liu, L. (1992), Orbital Mechanics of Artificial Earth Satellite, Higher Education Publishing, Beijing. (In Chinese)
8. Sang, J., Chen, L., Li, B., Du, J., Chen, J., Zhang, P. (2016). Development of space object orbit information software platform. *Spacecraft Environment Engineering.* 33(1): 1 – 6. (in Chinese)